Changes in peat chemistry associated with permafrost thaw increase greenhouse gas production

Suzanne B. Hodgkins[a,1], Malak M. Tfaily[a], Carmody K. McCalley[b], Tyler A. Logan[c], Patrick M. Crill[d], Scott R. Saleska[b], Virginia I. Rich[e], and Jeffrey P. Chanton[a,1]

[a]Department of Earth, Ocean, and Atmospheric Science, Florida State University, Tallahassee, FL 32306; [b]Department of Ecology and Evolutionary Biology, University of Arizona, Tucson, AZ 85721; [c]Abisko Scientific Research Station, Swedish Polar Research Secretariat, SE-981 07 Abisko, Sweden; [d]Department of Geological Sciences, Stockholm University, SE-106 91 Stockholm, Sweden; and [e]Department of Soil, Water and Environmental Science, University of Arizona, Tucson, AZ 85721

Edited by Nigel Roulet, McGill University, Montreal, Canada, and accepted by the Editorial Board March 7, 2014 (received for review August 1, 2013)

Carbon release due to permafrost thaw represents a potentially major positive climate change feedback. The magnitude of carbon loss and the proportion lost as methane (CH_4) vs. carbon dioxide (CO_2) depend on factors including temperature, mobilization of previously frozen carbon, hydrology, and changes in organic matter chemistry associated with environmental responses to thaw. While the first three of these effects are relatively well understood, the effect of organic matter chemistry remains largely unstudied. To address this gap, we examined the biogeochemistry of peat and dissolved organic matter (DOM) along a ∼40-y permafrost thaw progression from recently- to fully thawed sites in Stordalen Mire (68.35°N, 19.05°E), a thawing peat plateau in northern Sweden. Thaw-induced subsidence and the resulting inundation along this progression led to succession in vegetation types accompanied by an evolution in organic matter chemistry. Peat C/N ratios decreased whereas humification rates increased, and DOM shifted toward lower molecular weight compounds with lower aromaticity, lower organic oxygen content, and more abundant microbially produced compounds. Corresponding changes in decomposition along this gradient included increasing CH_4 and CO_2 production potentials, higher relative CH_4/CO_2 ratios, and a shift in CH_4 production pathway from CO_2 reduction to acetate cleavage. These results imply that subsidence and thermokarst-associated increases in organic matter lability cause shifts in biogeochemical processes toward faster decomposition with an increasing proportion of carbon released as CH_4. This impact of permafrost thaw on organic matter chemistry could intensify the predicted climate feedbacks of increasing temperatures, permafrost carbon mobilization, and hydrologic changes.

High-latitude soils in the Northern Hemisphere contain an estimated 1,400–1,850 petagrams (Pg) of carbon, of which ∼277 Pg is in peatlands within the permafrost zone (1, 2). This quantity of 277 Pg represents over one-third of the carbon stock in the atmosphere (*ca*. 800 Pg) (3). The fate of this carbon in a warming climate—i.e., the responses of net carbon balance and CH_4 emissions—is important in predicting climate feedbacks of permafrost thaw. Although northern peatlands are currently a net carbon sink, and have been since the end of the last glaciation, they are a net source of CH_4 (4, 5), emitting 0.046–0.09 Pg of carbon as CH_4 per year (4, 6, 7). Due to CH_4's disproportionate global warming potential (33× CO_2 for 1 kg CH_4 vs. 1 kg CO_2 at a 100-y timescale) (8), this is equivalent to 6–12% of annual fossil fuel emissions of CO_2 (8.7 Pg of C) (9). The thaw of permafrost peatlands may alter their CH_4 and CO_2 emissions due to mobilization of formerly frozen carbon, higher temperatures, altered redox conditions, and evolving organic matter chemistry. Changes in carbon emissions, and in CH_4 emission in particular, could have potentially significant climate impacts.

CH_4 is produced by two primary mechanisms (10–12), distinguishable by $\delta^{13}C$ values. The reduction of CO_2 with H_2 (hydrogenotrophic production) generally produces CH_4 more depleted in ^{13}C ($\delta^{13}C = -110$ to $-60‰$) than CH_4 produced by the cleavage of acetate into CH_4 and CO_2 ($\delta^{13}C = -70$ to $-30‰$) (10, 11, 13–15). Due to the coproduction or utilization of CO_2 during CH_4 production (10–12, 16, 17), $\delta^{13}C_{CH4}$ also depends on $\delta^{13}C_{CO2}$, so we use the more robust parameter α_C (10) to represent the isotopic separation between CH_4 and CO_2. Despite the two production pathways' stoichiometric equivalence (17), they are governed by different environmental controls (18). Distinguishing these controls and further mapping them is therefore essential for predicting future changes in CH_4 formation under changing environmental conditions. Several studies have suggested that the proportion of CH_4 produced by acetate cleavage relative to CO_2 reduction is likely to increase with increasing pH (19, 20) and organic matter reactivity (12, 14, 15), but direct evidence of the latter is lacking.

In this study, we tested the hypotheses that (*i*) organic matter reactivity increases with permafrost thaw due to thaw-induced subsidence and associated shifts in hydrology and plant community (21), and (*ii*) CH_4 production shifts from hydrogenotrophic to acetoclastic due to this increase in organic matter reactivity. We assessed organic matter reactivity along a distinct chronosequence of permafrost thaw stages with differing plant community and hydrology by performing anaerobic incubations of peat collected along this sequence. We then compared the results to peat and dissolved organic matter (DOM) chemical structure, as described by C/N ratios and Fourier transform infrared (FTIR) spectroscopy of peat and Fourier transform ion cyclotron resonance mass spectrometry

Significance

We address the effect of thawing permafrost, and attendant subsidence-induced shifts in hydrology and plant community structure, on CH_4 and CO_2 production potentials and mechanisms driven by changes in organic matter chemical composition in a thawing peatland complex. Advanced analytical characterization of peat and dissolved organic matter along the thaw progression indicated increasingly reduced organic matter experiencing greater humification rates, which were associated with higher relative CH_4 and CO_2 production potentials, increasing relative CH_4/CO_2 production ratios, and shifts from hydrogenotrophic to acetoclastic methanogenesis. The effects of this increase in organic matter reactivity with permafrost thaw could intensify the increases in CH_4 and CO_2 release already predicted due to increasing temperatures, permafrost carbon mobilization, and waterlogging-induced changes in redox conditions.

Author contributions: S.B.H., P.M.C., S.R.S., V.I.R., and J.P.C. designed research; S.B.H., M.M.T., C.K.M., T.A.L., V.I.R., and J.P.C. performed research; M.M.T., T.A.L., and J.P.C. contributed new reagents/analytic tools; S.B.H. and M.M.T. analyzed data; and S.B.H., M.M.T., P.M.C., V.I.R., and J.P.C. wrote the paper.

The authors declare no conflict of interest.

This article is a PNAS Direct Submission. N.R. is a guest editor invited by the Editorial Board.

[1]To whom correspondence may be addressed. E-mail: sbh10c@fsu.edu or jchanton@fsu.edu.

This article contains supporting information online at www.pnas.org/lookup/suppl/doi:10.1073/pnas.1314641111/-/DCSupplemental.

Table 1. Sites selected for study, in order of thaw stage; detailed descriptions of each site (with justification their positions in the thaw sequence) are given in Table S1

Site name	Habitat classification	Dominant vegetation	pH
PHS	Collapsed palsa	*E. vaginatum*, woody species	4.1
PHB	Collapsed palsa	*E. vaginatum*, floating *Sphagnum*	4.1
Bog1	Bog	*Sphagnum* spp.	4.2
SOS	Bog	*Sphagnum* spp.	4.0
S (triplicate cores)	Bog	*Sphagnum* spp.	4.2
EOS	Fen	*E. angustifolium*, *Sphagnum* spp.	4.8
E (triplicate cores)	Fen	*E. angustifolium*	5.8
Fen1	Fen	*C. rostrata*	6.0
Fen2	Fen	*E. angustifolium*	5.7

(FT-ICR MS) of DOM. Our study specifically addresses the effect of thawing permafrost, and its attendant shifts in hydrology and plant communities, on CH_4 and CO_2 production potentials and mechanisms, via changes in organic matter chemical composition (commonly referred to as organic matter "quality") in a thawing peatland complex.

Study Site and Habitat Classification

Stordalen Mire (68.35°N, 19.05°E) is a peat plateau in northern Sweden with a peat depth ranging from 1 to 3 m (22). The ground's thaw state and consequent relationship to the water table determine the plant community, which in turn determines organic matter composition (21). Detailed vegetation surveys and analyses of aerial photographs taken at Stordalen (22–24) have demonstrated that permafrost thaw between 1970 and 2000 has caused dry permafrost hummocks to decrease in area by 10%, giving way to wetter minerotrophic sites, which increased by 17% (24). These changes have been accompanied by shifts in plant community from shrubs and lichens in permafrost hummocks to *Sphagnum* spp. in wetter sites followed by evolution to tall graminoid species as thaw-induced subsidence increases (22–24). Our site selections are based on these studies, which provide direct evidence that at minimum, six of our sites (Table 1 and Table S1) were once palsa (sites named PHS, PHB, S, and E) or likely palsa (sites named Bog1 and Fen1) underlain by permafrost (22–24). Similar processes are known to occur in other Arctic peatlands, where permafrost thaw creates wet depressions that are colonized first by *Sphagnum* and then by sedge species as the ground collapses with increasing thaw (25–27).

For this study, habitats were classified as "palsa," "collapsed palsa," "bog," or "fen." The palsa, bog, and fen classifications correspond, respectively, to the dry ombrotrophic (I), combined semiwet and wet ombrotrophic (II and III), and tall graminoid minerotrophic (IV) classifications of Johansson et al. (22) and represent a thaw gradient of increasing active layer depth. To these we added the additional designation of collapsed palsa for recently thawed waterlogged thermokarst sinkholes surrounded by palsa. Vegetation in these collapsed palsa sites is generally more diverse than that in the other three habitats, ranging from woody shrubs and *Eriophorum vaginatum* where the water table is at or just below the peat surface to floating *Sphagnum* mats where the water table is at or above the peat surface. Over time, vegetation in collapsed palsa may shift toward domination by nonfloating *Sphagnum* spp. (more bog-like) or sedges (more fen-like). Although permafrost thaw does not necessarily progress through all of these stages—for instance, rapid thaw may create a collapsed palsa sinkhole, which subsequently becomes more like a bog or a fen, whereas more gradual thawing may skip the collapsed palsa stage and cause more gradual changes in vegetation—these stages represent a thaw progression based on the possible shifts in vegetation and hydrology. Following a temporal succession of apparent time since onset of thaw, the habitats are ordered: (*i*) palsa, (*ii*) collapsed palsa, (*iii*) bog, and (*iv*) fen.

We selected nine sites spanning the thaw progression from collapsed palsa to fen (Table 1 and Table S1). Intact palsa sites were not included in this study because their dry, aerobic status prevents meaningful comparison with other sites based on anaerobic incubations and DOM measurements. Previous measurements of CH_4 and CO_2 fluxes from palsas have shown that they produce negligible amounts or even consume ambient CH_4 (23, 28, 29) but are a net source of CO_2 (28).

Results

Thaw Increases Potential CH_4 and CO_2 Production. Anaerobic incubations (Fig. S1) reveal significant increases in potential CH_4 and CO_2 production and CH_4/CO_2 ratios along the thaw progression ($P < 0.0001$ for all of these trends) (Fig. 1 and Fig. S2).

Thaw Shifts Methanogenesis to the Acetoclastic Pathway. $\delta^{13}C$ and α_C of incubation CH_4 and CO_2 are shown in Fig. 2. Higher α_C (and more negative $\delta^{13}C_{CH4}$) indicates a higher proportion of hydrogenotrophic methanogenesis, whereas lower α_C (and less negative $\delta^{13}C_{CH4}$) implies more acetoclastic methanogenesis (10, 12). The incubations fall into two groups (Fig. 2*C*) with a significant ($P < 0.0001$) separation in α_C values: collapsed palsa and bog peat with α_C between 1.075 and 1.092, and fen peat with α_C between 1.048 and 1.062. This result suggests a distinct shift from hydrogenotrophic to acetoclastic methanogenesis along the thaw progression associated with increasing organic matter lability (Fig. 1 *A* and *B*) and increasing pH (Table 1). $\delta^{13}C_{CO2}$ (Fig. 2*B*)

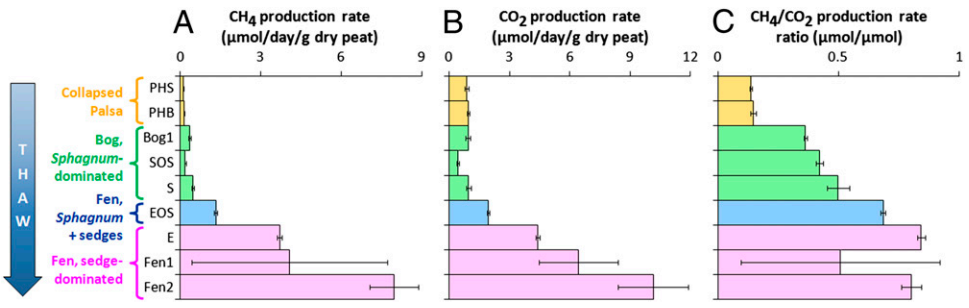

Fig. 1. CH_4 and CO_2 production rates in anaerobic incubations (±SE between replicates), which represent relative organic matter lability as potential decomposition rates. Samples are grouped into categories and placed in hypothesized order of permafrost thaw progression as described in Table 1 and Table S1. (*A*) CH_4 production rates, (*B*) CO_2 production rates, and (*C*) ratios of CH_4/CO_2 production.

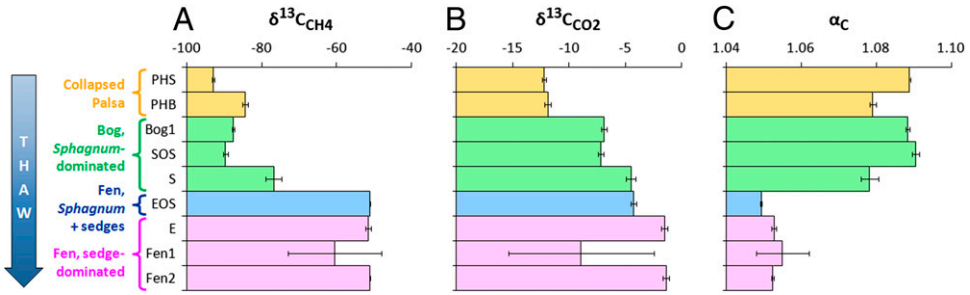

Fig. 2. Carbon isotopic composition of CH_4 and CO_2 produced in anaerobic incubations (±SE between replicates): (*A*) $\delta^{13}C_{CH4}$, (*B*) $\delta^{13}C_{CO2}$, and (*C*) α_C, defined as $(\delta^{13}C_{CO2} + 1{,}000)/(\delta^{13}C_{CH4} + 1{,}000)$. α_C and $\delta^{13}C_{CH4}$ imply a shift in methanogenesis from hydrogenotrophy to acetoclasty along the thaw gradient associated with increasing pH and organic matter lability. Increasing $\delta^{13}C_{CO2}$ is consistent with increasing CH_4/CO_2 production ratios (Fig. 1*C*) (17).

also increases along the thaw progression, consistent with the increasing CH_4/CO_2 ratio (Fig. 1*C*) and reflecting an increasing proportion of methanogenesis-derived CO_2 (17).

Peat C/N Ratios Reflect Plant Community Shifts. C/N ratios (by weight) of the peat used in the incubations are highest in bogs, intermediate in collapsed palsas, and lowest in fens (Fig. 3*A*). This trend is consistent with shifts in plant litter quality along the thaw sequence. Living plant samples of dominant Stordalen species collected at the Marcell Experimental Forest (northern Minnesota) showed a similar pattern in C/N ratios, from *E. vaginatum* (common in intact palsas, collapsed palsas, and bogs; C/N = 39 ± 24), through *Sphagnum* spp. (common in bogs; C/N = 46 ± 18), *Eriophorum angustifolium* (common in fens; C/N = 19 ± 0.4), and *Carex* spp. (common in fens; C/N = 25 ± 3).

Peat Becomes More Labile Across the Thaw Gradient. To investigate the structure of the peat organic matter, we used FTIR spectroscopy to examine: (*i*) surface peat (<10 cm, average ~3 cm); (*ii*) near-surface peat used in incubations, sampled just below the water table, examined preincubation (<22 cm, average ~11 cm); and (*iii*) deeper peat (24–35 cm, average ~25 cm) (Table S2). Whereas the spectra are generally similar between samples, the relative intensity of particular bands differs (Fig. 4), revealing the nature of chemical changes during peat development and humification (30). Along the thaw progression, carboxylic acid bands [1,720 cm^{-1} (31–34); Fig. 4*A*] weaken, likely because the fens' higher pH (Table 1) maintains organic acids as nonvisible carboxylate anions. Surface fen peat had more abundant polysaccharides [1,030–1,080 cm^{-1} (35)] and less abundant lignins [1,513–1,515 cm^{-1} (33)], aromatics [1,600–1,650 cm^{-1} (31)], and aliphatics [2,850 and 2,920 cm^{-1} (31)] than deep fen peat, indicating more cellulose (O-alkyl-C) plant material in the former vs. more decomposed, humified structures in the latter (Fig. 4*B*; less-pronounced differences were seen in bog and collapsed palsa peat).

To further identify the FTIR spectral differences between peat in different habitats, we calculated ratios of aliphatic, aromatic, and phenolic moieties to polysaccharides (Table S2), defined as humification indices (HI) (36) because they tend to increase with decomposition in soils. Across the sites, the surface and near-surface peat lacked consistent differences in HI; however, in the deep peat, fen HIs (except site E) were higher than collapsed palsa and bog HIs, suggesting more advanced decomposition in deep fen peat (Table S2). (In fen site E, remnant *Sphagnum* at depth resulted in an HI similar to deep bog samples, because HI reflects both source plant material and decomposition.) Consistent with increased decomposition with depth, most HIs were higher in deep than in surface peat (Table S2; see also Fig. 4*B*). This change can be quantified as a humification rate by calculating the ratio of deep to surface HI (24–35 cm vs. 0–10 cm), with higher ratios implying higher rates of humification through the soil column (i.e., faster decomposition over time). Humification rates with respect to all wavenumbers increased along the thaw progression, with the greatest increases occurring for the transformation of polysaccharides into aliphatic moieties (2,920 and 2,850 cm^{-1}) (Fig. 3*B*).

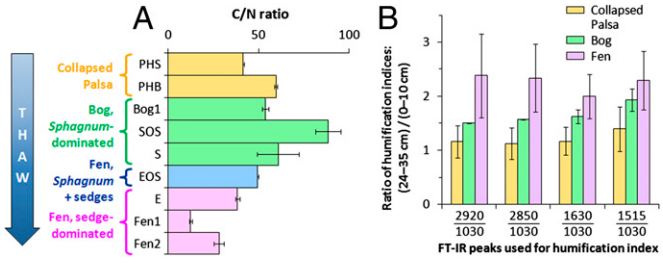

Fig. 3. Peat chemistry changes with thaw. (*A*) C/N weight ratios (±SE) of preincubation peat. (*B*) Ratios of deep (24–35 cm) to surface (<10 cm) peat HI for each site category (±SE), representing humification rates, for several wavenumbers (Fig. 4*B*) with respect to polysaccharides (1,030 cm^{-1}). The bog category excludes site S (which had no samples below 21 cm), and the fen category excludes site E (which had *Sphagnum* remains at depth).

DOM Chemistry Changes with Thaw. To investigate the structure of DOM, pore water samples spanning the thaw progression were analyzed by FT-ICR MS, of which representative bog (SOS site, 31 cm) and fen (E site, 25.5 cm) samples are shown (Fig. 5 and Fig. S3; Table 2). Peaks were assigned molecular formulas, taking into account C, H, O, N, and S (total 21,114 compounds; 11,527 bog and 9,587 fen), which were classified based on their N and S content and H/C and O/C ratios (Table 2). Sixty-four percent of compounds (13,436/21,114) were present in both samples (i.e., matching). To visualize differences in DOM composition, compounds that were unique to each sample (i.e., nonmatching) are plotted by their H/C vs. O/C ratios and molecular size (Fig. 5).

DOM compositional differences are clear between bog and fen sites. In the SOS/E site comparison (Fig. 5 and Fig. S3; Table 2), this is despite E's presence of remnant *Sphagnum* at depth, revealing that DOM at depth (unlike solid peat) is shaped by surface vegetation (39) even when buried remnants of older vegetation are present. Two distinct compound classes can be seen in both samples (Fig. 5*A*): class 1, occupying most of the plot area and representing various aliphatics, lignins, and tannins, and class 2 in the lower left-hand corner (O/C = 0–0.4, H/C = 0–0.8) representing condensed aromatic structures (37). Within both classes, O/C ratios are lower in fen than in bog DOM. Specifically, fen DOM contained more lipid-, other low-O/C-, protein- and amino sugar- (AS), and lignin-like compounds, whereas bog DOM contained more condensed aromatic and tannin-like compounds (Table 2 and Fig. 5*A*) (37). Fen DOM also had a lower average molecular size than bog DOM (Fig. 5*B*).

To characterize the oxidation states and unsaturation of the compounds comprising DOM, the double-bond equivalence (DBE), i.e., the total number of double bonds and aliphatic rings in each molecular formula, was calculated. The DBE distribution in bog DOM is skewed toward higher values compared with fen DOM (Fig. S3*A*), indicating that bog DOM is more unsaturated overall. To characterize C=C bonds and rings, DBE−O was calculated as the number of oxygen atoms subtracted from DBE

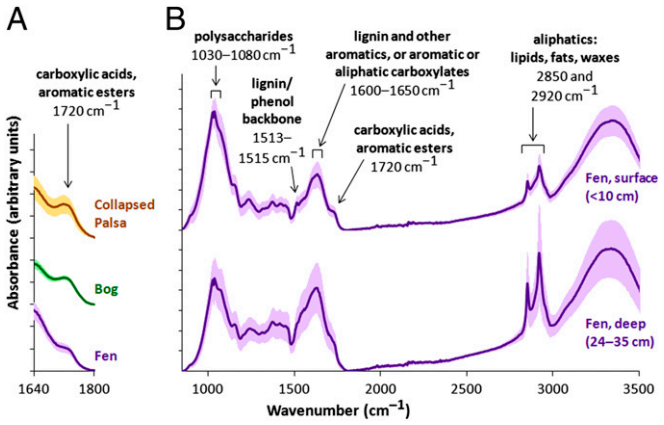

Fig. 4. Average peat FTIR absorption spectra, with between-site SEs as shaded areas. Spectra are stacked (i.e., absorbance = 0 at each apparent baseline) and sized to the same vertical scale. (*A*) Organic acids in incubated peat samples (preincubation) decrease with thaw from collapsed palsas ($n = 2$) to bogs ($n = 3$) to fens (including both sedge only and *Sphagnum* + sedge; $n = 4$). (*B*) In fens (excluding site E, which had *Sphagnum* remains at depth), humification leads to spectral changes between surface ($n = 3$) and deep ($n = 3$) peat. References for wavenumbers: see *Results, Peat Becomes More Labile Across the Thaw Gradient*.

under the assumption that most DOM oxygen is bound to carbon by a double bond (40, 41). In contrast with DBE, the DBE–O distribution is lower in bog than in fen DOM (Fig. S3*B*). This difference between the DBE and DBE–O distributions indicates that bog DOM contains more hydrophilic, oxygen-rich compounds than fen DOM, and that a larger portion of the unsaturation in bog DOM is due to C=O bonds (mostly from carboxylic acid) than in fen DOM (41, 42). The higher oxygen content of bog DOM, as evidenced by both its DBE/DBE–O distributions and its higher O/C ratios relative to fen DOM, indicate that bog DOM has a higher oxidation state than fen DOM.

Discussion

The increase in relative peat CH_4 and CO_2 production potentials (Fig. 1 *A* and *B*) along the thaw gradient when incubated under identical temperature and water saturation indicates an increase in organic matter lability. We propose three primary causes for this increase, all of which are tied to the changes in plant community associated with permafrost thaw: (*i*) increasing pH causes loss of organic acids that would otherwise inhibit microbial decomposition; (*ii*) decreasing peat C/N ratios increase organic matter quality by providing more abundant nitrogen; and (*iii*) increasing protein-like (and perhaps also relatively labile lipid-like) compounds in DOM may act as high-quality substrates for microbes. These changes can be directly observed in the chemical structure of peat and DOM along the thaw progression.

The types of compounds comprising organic matter help define its lability. For example, undissociated organic acids, particularly sphagnum acid and other *Sphagnum*-derived phenolics (43, 44), inhibit organic matter decay. The apparent increase in lability across the gradient could thus be due to a decrease in organic acids (Fig. 4*A*) driven by changing plant inputs and increasing pH (Table 1 and Table S1). However, pH's effect on decomposition (both directly through impacts on microbial activity and indirectly via shifting organic acids to their less inhibitory anionic forms) is unlikely to be the sole process governing decomposition rates in this system, given Ye et al.'s (45) demonstration that incubating bog peat at fen-typical pH did not stimulate fen-like CH_4 production to the levels seen in fen peat. Phenolic abundance may also decrease along the thaw sequence due to the enzymatic latch mechanism (46), whereby the enzyme phenol oxidase (which degrades phenolic compounds) depends on bimolecular oxygen availability. In fens, vascular plant roots may transport oxygen into the soil, where it activates phenol oxidase and thereby decreases the concentration of decomposition-inhibiting phenolics. Decreasing C/N ratios (Fig. 3*A*), driven by thaw-associated changes in plant community (from *E. vaginatum* and *Sphagnum* spp. to *E. angustifolium* and *Carex rostrata*) that lower the organic matter C/N ratio, may also increase organic matter lability by decreasing nitrogen limitation for decomposers.

Whereas the solid-phase peat represents an important substrate for decomposition, a large proportion of CH_4 and CO_2 production uses materials in the dissolved phase (39). This is particularly true in fens due to fen DOM's high lability (relative to bog DOM), such that the majority of fen respiration products is derived from DOM decomposition (39). We therefore analyzed DOM chemistry and reactivity in addition to peat chemistry and reactivity. The DOM chemical structure was markedly different between bog and fen (Fig. 5 and Fig. S3; Table 2), shaped in part by different plant source material. Decay-resistant tannins from *Sphagnum* were abundant in the bog, whereas the fen had a higher proportion of comparatively labile protein- and fatty-acid-like compounds possibly originating as sedge root exudates.

In addition to organic matter compositional differences that directly affect its lability, there are also differences indicating the degree of decomposition. Ratios of HI in deep vs. surface peat, which represent decomposition rates through the soil column, indicate that decomposition rates increase along the thaw progression (Fig. 3*B*). Analogous to the fens' higher solid-phase humification rates with respect to the accumulation of both lignin- and lipid-like moieties (Fig. 3*B*), fen DOM also has a higher percentage of dissolved lignin- and lipid-like compounds (some of which are recalcitrant and can accumulate) than bog DOM (Table 2), consistent with more advanced decomposition. Fen DOM also has a smaller average molecular size than bog DOM (Fig. 5*B*). This result is consistent with the size reactivity model, in which high molecular weight DOM is hydrolyzed into low molecular weight DOM, causing small refractory compounds to accumulate (38). Furthermore, because microbial biomass includes abundant lipid- and protein-like substances, these

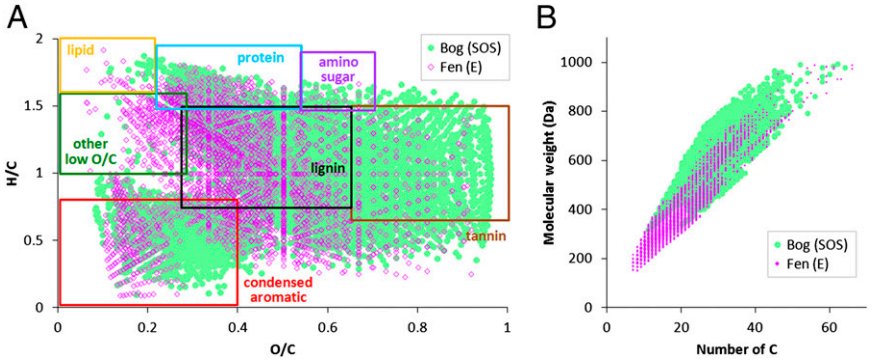

Fig. 5. Analysis of molecular formulas found in DOM in representative bog (site SOS, 31 cm, green circles) and fen (site E, 25.5 cm, purple diamonds) samples. (*A*) van Krevelen diagram of nonmatching formulas (those not shared between samples) in bog vs. fen DOM, labeled with the specific compound classes expected to occur in each region (37). Each point represents one molecular formula present in one sample, plotted by its O/C and H/C ratio. (*B*) Molecular size distribution of nonmatching formulas. Smaller molecules in fen DOM indicate more advanced decay compared with bog DOM (38).

Table 2. Abundance of different types of formulas based on elemental composition (containing CHO only; CHON only; CHOS only; and CHONS) and compound class (described in the van Krevelen diagram; Fig. 5*A*)

Sample	No. of formulas	CHO %m (±1.6)	CHON %m (±1.2)	CHOS %m (±0.5)	CHONS %m (±0.1)	Lipid-like %m (±0.0)	Protein- and AS-like %m (±0.4)	Other low-O/C* %m (±0.8)	Lignin-like %m (±1.3)	Tannin-like %m (±0.9)	Condensed aromatics %m (±0.2)
All formulas:											
Bog (SOS)	11,527	88.9	7.6	2.4	1.1	0.0	2.2	0.2	45.9	40.2	2.3
Fen (E)	9,587	79.7	9.2	10.3	0.8	2.6	5.3	4.0	59.9	20.2	1.0
Nonmatching formulas:											
Bog (SOS)	4,809	72.7	18.2	3.2	5.9	0.2	2.9	0.3	40.9	32.2	15.4
Fen (E)	2,869	69.3	6.9	22.0	1.9	9.7	7.7	13.9	63.0	4.5	2.7

Abundances are given as %m, which represents the combined relative abundance of all formulas in each class as a percentage of the total abundance of all formulas. SEs for each category are based on a parallel analysis of replicate samples collected at the same depth and time.
*Peaks in the region with $1 \leq H/C \leq 1.6$ and $0 \leq O/C \leq 0.29$, representing low-O compounds similar to lipids but with lower H/C (Fig. 5*A*).

categories, as well as the unknown low-O/C category (which appears in the same general region of the van Krevelen plot; Fig. 5*A*), may represent microbial biomass. Higher microbial biomass in the fen is likely associated with higher microbial activity (47), so this result is consistent with the higher CH_4 and CO_2 production potentials (Fig. 1 *A* and *B*) and humification rates (Fig. 3*B*) observed in fens relative to bogs.

The increase in relative CH_4/CO_2 production ratios along the thaw progression has several possible explanations. Anaerobic CH_4 oxidation (48, 49), if present, may be more pronounced in collapsed palsa and bog peat than in fen peat, but because CH_4 oxidation tends to enrich the $\delta^{13}C$ of residual CH_4 (50) whereas the $\delta^{13}C_{CH4}$ values in bog and collapsed palsa peat were relatively depleted (Fig. 2*A*), this explanation seems unlikely. More plausible reasons for the observed CH_4/CO_2 ratios involve pH and organic matter oxidation state. Ye et al. (45) demonstrated that CH_4/CO_2 production ratios increase with pH, which suggests that the low pH of the bog and collapsed palsa habitats may selectively inhibit CH_4 more than CO_2 production. Methanogenesis in collapsed palsa and bog peat may also be inhibited by non-O_2 electron acceptors, particularly humic acids (51–54), whereas fen DOM's lower oxidation state (Fig. 5*A* and Fig. S3) may translate to lower humic acid electron-accepting capacity. The lower O/C ratios in fen DOM could also support higher relative CH_4/CO_2 production ratios based on its stoichiometry, which supports the direct conversion of more DOM to CH_4 instead of CO_2 (55, 56). Finally, the low CH_4/CO_2 ratios in bogs and collapsed palsas may reflect diversion of reduced decay products into microbial biomass (anabolism) instead of CH_4 (catabolism).

Because the peat was incubated at a higher temperature (22 °C) than generally found at the incubated depths (<15 °C), it is possible that the incubation CH_4/CO_2 production ratios could be higher than field ratios due to rapid consumption of alternate electron acceptors in the higher-temperature, closed incubations (57). However, gas production was linear over the incubations (Fig. S1), and Lupascu et al. (29) found similar relative differences in methanogenesis between *Sphagnum* and sedge peat from Stordalen when incubated at 4 °C, 14 °C, and 24 °C. The lower CH_4/CO_2 ratios in the early part of the thaw sequence are also consistent with bog DOM's higher oxidation state and organic oxygen content relative to fen DOM (Fig. 5*A* and Fig. S3). The incubations thus provide a useful proxy for relative field CH_4/CO_2 ratios.

Combined with the increases in organic matter lability as revealed by the incubations, as well as the more advanced decay state of fen peat and DOM relative to bog and collapsed palsa peat and bog DOM as revealed by FTIR and FT-ICR MS, the shift from hydrogenotrophic to acetoclastic methanogenesis with thaw (Fig. 2) is consistent with the understanding that these shifts are associated with increasing organic matter lability (12, 14, 15). A likely mechanism for this effect is the loss of organic acids along the thaw progression (Fig. 4*A*) driven by increasing pH (Table 1), because hydrogenotrophic methanogens are generally more acid-tolerant than acetoclastic methanogens (18, 20, 58).

Conclusions

Based on increases in CH_4 and CO_2 production potentials across the permafrost thaw progression, organic matter lability appears to increase significantly with thaw, subsidence, and resulting changes in vegetation (i.e., up to 10–15× more $CH_4 + CO_2$ production in incubations of fen peat compared with collapsed palsa peat; Fig. 1 *A* and *B*). In addition to the overall increase in decomposition potential, the incubations also showed a five- to sixfold increase in the relative proportion of decomposition by methanogenesis (Fig. 1*C*) along with a shift from hydrogenotrophic to acetoclastic CH_4 production (Fig. 2). Although controlled laboratory incubations and organic matter characterizations of targeted field samples cannot be directly upscaled to absolute field CH_4 and CO_2 production, the increases in in situ organic matter quality and decomposition rates (as indicated by C/N ratios and FTIR of peat and FT-ICR MS of DOM) suggest that the trends seen in the incubations are likely to translate into relative increases in field CH_4 and CO_2 production rates and CH_4/CO_2 ratios along the thaw progression, which are likely to be further enhanced by increased graminoid-mediated gas transport in fens (59).

As the Arctic warms, peat is expected to release more CH_4 and CO_2 as permafrost thaws and exposes more peat, and as peat experiences faster decomposition due to increasing temperatures. The production of CH_4 relative to CO_2 is also likely to increase due to increasing anaerobic conditions caused by peat waterlogging associated with thaw and subsidence. Our results suggest that estimates of CH_4 climate feedbacks based on these effects alone are likely to be conservative: as permafrost thaws, overall carbon release, as well as the proportion released as CH_4, is likely to increase on a per-volume basis as thaw-induced subsidence and shifts in plant community increase organic matter lability and favor increasingly methanogenic conditions.

Materials and Methods

Incubations were performed in the dark under water-saturated, anaerobic conditions with a N_2 headspace at 22 °C. Although this temperature is higher than those likely to occur at ~10-cm depth in the field, it is common practice to incubate samples at a temperature higher than in situ to observe significant increases in gas production at the timescales used for laboratory experiments (21, 60–63). The results thus represent potential CH_4 and CO_2 production rates (21), which are evaluated relative to one another to assess changes in organic matter lability along the thaw sequence.

For additional details on incubations, C/N ratios, FTIR, and FT-ICR MS, see *SI Materials and Methods*.

ACKNOWLEDGMENTS. We thank Tyler Mauney for incubation preparation, Claire Langford for CH_4 and CO_2 concentration and $\delta^{13}C$ analysis, Alejandra Mickle for C/N analysis, David Podgorski for FT-ICR MS, and the Abisko

Scientific Research Station for providing infrastructure for sampling. This research was funded by the US Department of Energy Office of Biological and Environmental Research under the Genomic Science (Award DE-SC0004632) and Terrestrial Ecosystems Science (Contract ER65245) programs.

1. Schuur EAG, et al. (2008) Vulnerability of permafrost carbon to climate change: implications for the global carbon cycle. *Bioscience* 58(8):701–714.
2. McGuire AD, et al. (2009) Sensitivity of the carbon cycle in the Arctic to climate change. *Ecol Monogr* 79(4):523–555.
3. Houghton RA (2007) Balancing the global carbon budget. *Annu Rev Earth Planet Sci* 35:313–347.
4. Gorham E (1991) Northern peatlands: Role in the carbon cycle and probable responses to climatic warming. *Ecol Appl* 1(2):182–195.
5. Whiting GJ, Chanton JP (2001) Greenhouse carbon balance of wetlands: Methane emission versus carbon sequestration. *Tellus B Chem Phys Meteorol* 53(5):521–528.
6. Matthews E, Fung I (1987) Methane emission from natural wetlands: Global distribution, area, and environmental characteristics of sources. *Global Biogeochem Cycles* 1(1):61–86.
7. Crill PM, et al. (1988) Methane flux from Minnesota peatlands. *Global Biogeochem Cycles* 2(4):371–384.
8. Shindell DT, et al. (2009) Improved attribution of climate forcing to emissions. *Science* 326(5953):716–718.
9. Boden TA, Marland G, Andres RJ (2012) Global, regional, and national fossil-fuel CO_2 emissions. Carbon Dioxide Information Analysis Center (CDIAC). Available at http://dx.doi.org/10.3334/CDIAC/00001_V2012. Accessed December 5, 2012.
10. Whiticar MJ, Faber E, Schoell M (1986) Biogenic methane formation in marine and freshwater environments: CO_2 reduction *vs.* acetate fermentation—Isotope evidence. *Geochim Cosmochim Acta* 50(5):693–709.
11. Whiticar MJ (1999) Carbon and hydrogen isotope systematics of bacterial formation and oxidation of methane. *Chem Geol* 161(1-3):291–314.
12. Chanton JP, Chasar LC, Glaser P, Siegel D (2005) *Stable Isotopes and Biosphere-Atmosphere Interactions, Physiological Ecology Series*, eds Flanagan LB, Ehleringer JR, Pataki DE (Elsevier Academic, San Diego), pp 85–105.
13. Sugimoto A, Wada E (1993) Carbon isotopic composition of bacterial methane in a soil incubation experiment: Contributions of acetate and CO_2/H_2. *Geochim Cosmochim Acta* 57(16):4015–4027.
14. Hornibrook ERC, Longstaffe FJ, Fyfe WS (1997) Spatial distribution of microbial methane production pathways in temperate zone wetland soils: Stable carbon and hydrogen isotope evidence. *Geochim Cosmochim Acta* 61(4):745–753.
15. Hornibrook ERC, Longstaffe FJ, Fyfe WS (2000) Evolution of stable carbon isotope compositions for methane and carbon dioxide in freshwater wetlands and other anaerobic environments. *Geochim Cosmochim Acta* 64(6):1013–1027.
16. Shoemaker JK, Schrag DP (2010) Subsurface characterization of methane production and oxidation from a New Hampshire wetland. *Geobiology* 8(3):234–243.
17. Corbett JE, et al. (2013) Partitioning pathways of CO_2 production in peatlands with stable carbon isotopes. *Biogeochemistry* 114(1-3):327–340.
18. Hines ME, Duddleston KN, Rooney-Varga JN, Fields D, Chanton JP (2008) Uncoupling of acetate degradation from methane formation in Alaskan wetlands: Connections to vegetation distribution. *Glob Biogeochem Cycles* 22(2):GB2017.
19. Hines ME, Duddleston KN (2001) Carbon flow to acetate and C_1 compounds in northern wetlands. *Geophys Res Lett* 28(22):4251–4254.
20. Kotsyurbenko OR, et al. (2007) Shift from acetoclastic to H_2-dependent methanogenesis in a West Siberian peat bog at low pH values and isolation of an acidophilic *Methanobacterium* strain. *Appl Environ Microbiol* 73(7):2344–2348.
21. Turetsky MR (2004) Decomposition and organic matter quality in continental peatlands: The ghost of permafrost past. *Ecosystems (NY)* 7(7):740–750.
22. Johansson T, et al. (2006) Decadal vegetation changes in a northern peatland, greenhouse gas fluxes and net radiative forcing. *Glob Change Biol* 12(12):2352–2369.
23. Christensen TR, et al. (2004) Thawing sub-arctic permafrost: Effects on vegetation and methane emissions. *Geophys Res Lett* 31(4):L04501.
24. Malmer N, Johansson T, Olsrud M, Christensen TR (2005) Vegetation, climatic changes and net carbon sequestration in a North-Scandinavian subarctic mire over 30 years. *Glob Change Biol* 11(11):1895–1909.
25. Zoltai SC (1993) Cyclic development of permafrost in the peatlands of Northwestern Alberta, Canada. *Arct Alp Res* 25(3):240–246.
26. Vitt DH, Halsey LA, Zoltai SC (1994) The bog landforms of continental western Canada in relation to climate and permafrost patterns. *Arct Alp Res* 26(1):1–13.
27. Jorgenson MT, Racine CH, Walters JC, Osterkamp TE (2001) Permafrost degradation and ecological changes associated with a warming climate in central Alaska. *Clim Change* 48(4):551–579.
28. Bäckstrand K, et al. (2010) Annual carbon gas budget for a subarctic peatland, Northern Sweden. *Biogeosciences* 7(1):95–108.
29. Lupascu M, Wadham JL, Hornibrook ERC, Pancost RD (2012) Temperature sensitivity of methane production in the permafrost active layer at Stordalen, Sweden: A comparison with non-permafrost northern wetlands. *Arct Antarct Alp Res* 44(4):469–482.
30. Silamiķele I, et al. (2010) in *Mires and Peat*, ed Kļaviņ M (University of Latvia Press, Rīga, Latvia), pp 71–95. Available at www.lu.lv/fileadmin/user_upload/lu_portal/projekti/vpp/kuudra/Miresandpeat/mires-peat_71-95.pdf. Accessed July 31, 2013.
31. Niemeyer J, Chen Y, Bollag J-M (1992) Characterization of humic acids, composts, and peat by diffuse reflectance Fourier-transform infrared spectroscopy. *Soil Sci Soc Am J* 56(1):135–140.
32. Haberhauer G, Rafferty B, Strebl F, Gerzabek MH (1998) Comparison of the composition of forest soil litter derived from three different sites at various decompositional stages using FTIR spectroscopy. *Geoderma* 83(3-4):331–342.
33. Cocozza C, D'Orazio V, Miano TM, Shotyk W (2003) Characterization of solid and aqueous phases of a peat bog profile using molecular fluorescence spectroscopy, ESR and FT-IR, and comparison with physical properties. *Org Geochem* 34(1):49–60.
34. Gondar D, Lopez R, Fiol S, Antelo JM, Arce F (2005) Characterization and acid–base properties of fulvic and humic acids isolated from two horizons of an ombrotrophic peat bog. *Geoderma* 126(3-4):367–374.
35. Grube M, Lin JG, Lee PH, Kokorevicha S (2006) Evaluation of sewage sludge-based compost by FT-IR spectroscopy. *Geoderma* 130(3-4):324–333.
36. Broder T, Blodau C, Biester H, Knorr KH (2012) Peat decomposition records in three pristine ombrotrophic bogs in southern Patagonia. *Biogeosciences* 9(4):1479–1491.
37. Sleighter RL, Hatcher PG (2007) The application of electrospray ionization coupled to ultrahigh resolution mass spectrometry for the molecular characterization of natural organic matter. *J Mass Spectrom* 42(5):559–574.
38. Burdige DJ, Gardner KG (1998) Molecular weight distribution of dissolved organic carbon in marine sediment pore waters. *Mar Chem* 62(1-2):45–64.
39. Chanton JP, et al. (2008) Radiocarbon evidence for the importance of surface vegetation on fermentation and methanogenesis in contrasting types of boreal peatlands. *Glob Biogeochem Cycles* 22(4):GB4022.
40. Gonsior M, et al. (2009) Photochemically induced changes in dissolved organic matter identified by ultrahigh resolution Fourier transform ion cyclotron resonance mass spectrometry. *Environ Sci Technol* 43(3):698–703.
41. Tfaily MM, Podgorski DC, Corbett JE, Chanton JP, Cooper WT (2011) Influence of acidification on the optical properties and molecular composition of dissolved organic matter. *Anal Chim Acta* 706(2):261–267.
42. Tfaily MM, Hodgkins S, Podgorski DC, Chanton JP, Cooper WT (2012) Comparison of dialysis and solid-phase extraction for isolation and concentration of dissolved organic matter prior to Fourier transform ion cyclotron resonance mass spectrometry. *Anal Bioanal Chem* 404(2):447–457.
43. Mellegård H, Stalheim T, Hormazabal V, Granum PE, Hardy SP (2009) Antibacterial activity of sphagnum acid and other phenolic compounds found in *Sphagnum papillosum* against food-borne bacteria. *Lett Appl Microbiol* 49(1):85–90.
44. Zaitseva N (2009) A polysaccharide extracted from *Sphagnum* moss as antifungal agent in archaeological conservation. Master's thesis (Queen's University, Kingston, Ontario, Canada). Available at http://hdl.handle.net/1974/5392. Accessed April 30, 2013.
45. Ye R, et al. (2012) pH controls over anaerobic carbon mineralization, the efficiency of methane production, and methanogenic pathways in peatlands across an ombrotrophic–minerotrophic gradient. *Soil Biol Biochem* 54:36–47.
46. Freeman C, Ostle N, Kang H (2001) An enzymic 'latch' on a global carbon store. *Nature* 409(6817):149.
47. Brake M, Höper H, Joergensen RG (1999) Land use-induced changes in activity and biomass of microorganisms in raised bog peats at different depths. *Soil Biol Biochem* 31(11):1489–1497.
48. Blazewicz SJ, Petersen DG, Waldrop MP, Firestone MK (2012) Anaerobic oxidation of methane in tropical and boreal soils: Ecological significance in terrestrial methane cycling. *J Geophys Res Biogeosci* 117(G2):G02033.
49. Gupta V, et al. (2013) Stable isotopes reveal widespread anaerobic methane oxidation across latitude and peatland type. *Environ Sci Technol* 47(15):8273–8279.
50. Whiticar MJ, Faber E (1986) Methane oxidation in sediment and water column environments—Isotope evidence. *Org Geochem* 10(4-6):759–768.
51. Lovley DR, Coates JD, Blunt-Harris EL, Phillips EJP, Woodward JC (1996) Humic substances as electron acceptors for microbial respiration. *Nature* 382(6590):445–448.
52. Heitmann T, Goldhammer T, Beer J, Blodau C (2007) Electron transfer of dissolved organic matter and its potential significance for anaerobic respiration in a northern bog. *Glob Change Biol* 13(8):1771–1785.
53. Keller JK, Bridgham SD (2007) Pathways of anaerobic carbon cycling across an ombrotrophic-minerotrophic peatland gradient. *Limnol Oceanogr* 52(1):96–107.
54. Blodau C, Deppe M (2012) Humic acid addition lowers methane release in peats of the Mer Bleue bog, Canada. *Soil Biol Biochem* 52:96–98.
55. Symons GE, Buswell AM (1933) The methane fermentation of carbohydrates. *J Am Chem Soc* 55(5):2028–2036.
56. Nilsson M, Öquist M (2009) *Carbon Cycling in Northern Peatlands, Geophysical Monograph Series*, eds Baird AJ, Belyea LR, Comas X, Reeve AS, Slater LD (American Geophysical Union, Washington, DC), pp 131–144.
57. van Hulzen JB, Segers R, van Bodegom PM, Leffelaar PA (1999) Temperature effects on soil methane production: An explanation for observed variability. *Soil Biol Biochem* 31(14):1919–1929.
58. Horn MA, Matthies C, Küsel K, Schramm A, Drake HL (2003) Hydrogenotrophic methanogenesis by moderately acid-tolerant methanogens of a methane-emitting acidic peat. *Appl Environ Microbiol* 69(1):74–83.
59. Chanton JP (2005) The effect of gas transport on the isotope signature of methane in wetlands. *Org Geochem* 36(5):753–768.
60. Glenn S, Heyes A, Moore T (1993) Carbon dioxide and methane fluxes from drained peat soils, southern Quebec. *Global Biogeochem Cycles* 7(2):247–257.
61. Blodau C, Moore TR (2003) Experimental response of peatland carbon dynamics to a water table fluctuation. *Aquat Sci* 65(1):47–62.
62. Blodau C, Basiliko N, Moore TR (2004) Carbon turnover in peatland mesocosms exposed to different water table levels. *Biogeochemistry* 67(3):331–351.
63. Lee H, Schuur EAG, Inglett KS, Lavoie M, Chanton JP (2012) The rate of permafrost carbon release under aerobic and anaerobic conditions and its potential effects on climate. *Glob Change Biol* 18(2):515–527.

Supporting Information

Hodgkins et al. 10.1073/pnas.1314641111

SI Materials and Methods

Sampling. Nine sites (Table 1 and Table S1) spanning the thaw progression from collapsed palsa to fen were selected for study. Between June 13 and June 16, 2011, peat was gathered with an 11-cm-diameter homemade circular push corer at all sites except the PHS and Fen1 sites, at which peat was gathered with a 10 cm × 10-cm square Wardenaar corer (Eijkelkamp). All sites were cored singly except S and E, which were cored in triplicate to capture spatial heterogeneity. Cores were divided into sections 3–10 cm thick, and the sections were placed into plastic bags and stored at 4 °C (the approximate peat temperature in the field) until analysis.

Before coring, pore water for pH and Fourier transform ion cyclotron resonance mass spectrometry (FT-ICR MS) was collected in the field by suction through a home-built 0.5-cm-diameter stainless steel tube connected to a 60-mL plastic syringe. pH was measured on-site with an Oakton Waterproof pHTestr 10 (Eutech Instruments). For FT-ICR MS, pore water was filtered through 0.7-μm Whatman GF/F glass microfiber filters into amber polycarbonate bottles and frozen within 8 h of collection until analysis.

Incubations. From each core, a section of surficial peat below the water table (Table S1) was selected for incubation. Three replicates were prepared for each site except for Fen1, which only had enough peat for two replicates. For sites with triplicate cores (S and E), each incubation replicate was taken from a separate core replicate, so the averages and SEs from these sites correspond with the averages and SEs across all three cores.

For each incubation replicate, 12–20 g of peat was placed in preweighed 100-mL borosilicate glass serum bottles (Wheaton, part number 223747) (actual volume to neck ∼120 mL), weighed, and covered with 40 mL of deionized water that had previously been degassed by bubbling N_2 through the water for 20 min. The final volume of peat plus water was enough to leave about 50–65% headspace volume in the bottles. The bottles were capped with 20-mm blue chlorobutyl septum stoppers (Bellco Glass, part number 2048–11800) and crimped with Supelco aluminum crimp seals (Sigma-Aldrich, part number 27230-U). Each vial had the headspace flushed with N_2 for 30 s, was shaken for 30 s, and had the headspace flushed again for 30 s. We performed a 25-d preincubation of vials in the dark at 22 °C to allow microbial elimination of any remaining oxygen or other electron acceptors introduced during processing, thus establishing methanogenic conditions. At the end of the preincubation, any CH_4 and CO_2 produced during the preincubation were removed by shaking the vials and flushing them with N_2 until additional shaking and flushing caused no further reduction in CH_4 and CO_2 concentrations. This procedure entailed shaking and flushing each vial a total of 5 times (30 s for each shaking, 30 s for the first two flushings, 60 s for the third flushing, and 3 min for the final two flushings), with maximum removal achieved after the first three shakings and flushings. Concentrations were determined by analysis on a Shimadzu GC-8A gas chromatograph with a methanizer and a flame ionization detector. After maximum removal, headspace CH_4 and CO_2 concentrations were <0.1% and <0.5% by volume, respectively; these concentrations were small compared to the later buildup in CH_4 and CO_2 during the main incubations (Fig. S1 *A*–*D*). At the end of the final flushing, enough N_2 was left in each vial to create a headspace pressure of 5–7 psi above atmospheric pressure as determined by a home-built needle-insertion pressure gauge. The end of the final flushing was defined as the incubation start time.

Vials were incubated at 22 °C in the dark for 62 d. One day following the incubation start date, and at least every 14 d thereafter, the headspace was analyzed for CH_4 and CO_2 concentrations and $\delta^{13}C$. Before each measurement, the incubation vials were shaken for 30 s, and the headspace pressures were measured. For determination of CH_4 and CO_2 concentrations and $\delta^{13}C$, headspace subsamples between 10 and 250 μL (depending on concentration) were directly injected into a continuous-flow Hewlett-Packard 5890 gas chromatograph (Agilent Technologies) at 35 °C coupled to a Finnigan MAT Delta S isotope ratio mass spectrometer via a Conflo IV interface system (Thermo Scientific) (GC-IRMS). Stable carbon isotope ratios ($^{13}C/^{12}C$) were expressed as $\delta^{13}C$ relative to the Pee Dee Belemnite (PDB) standard, where $\delta^{13}C = (R_{sample}/R_{standard} - 1) \times 1000$, and R_{sample} and $R_{standard}$ are the $^{13}C/^{12}C$ ratios in the sample and the PDB standard, respectively.

At the end of the incubation period and immediately following the final CH_4 and CO_2 analysis, samples were acidified with 2 mL of degassed 20% H_3PO_4 (excess) so that any dissolved inorganic carbon (DIC) that was still in the liquid phase could enter the headspace, and the samples were then analyzed again so that any changes in headspace CO_2 concentration or $\delta^{13}C$ could be determined. Acidification increased the headspace CO_2 concentration by >1% (the average relative error of the GC-IRMS concentration measurements) in only six of the incubations, all of them sedge fen peat with pH ≥ 5.7; consequently, a single replicate was measured for each of the bog and collapsed palsa sites (all of which had pH ≤ 4.2). Incubations that experienced no significant change in headspace CO_2 concentration (≤1%) with acidification also experienced negligible change in $\delta^{13}C_{CO2}$ (≤0.5‰). However, among the incubations that experienced >1% increase in headspace CO_2 concentration with acidification, $\delta^{13}C_{CO2}$ values also increased by up to 1.7‰.

Following the postacidification analysis of changes in CO_2 concentrations and $\delta^{13}C$, the sample vials were uncapped, dried at 60 °C until completely dry (∼60 d), and weighed.

Incubation Calculations. For CH_4, the total amount in the vial equals the amount of CH_4 in the headspace (based on an ideal gas law calculation) plus the amount of dissolved CH_4, which is calculated based on Henry's law:

$$n_{CH_4} = \frac{\chi_{CH_4} P (V_{vial} - V_{water})}{RT} + \chi_{CH_4} P V_{water} k_H, \qquad [S1]$$

where n_{CH_4} is the total amount of CH_4 in the vial (mol); χ_{CH_4} is the mole fraction in the headspace; P is the headspace pressure (atm); V_{vial} is the total vial volume (L); V_{water} is the volume of the combined peat and water (L), which is assumed (for simplification) to be mostly water; R is the gas constant ($L \cdot atm \cdot mol^{-1} \cdot K^{-1}$); T is the ambient temperature (K); and k_H is the Henry's law constant for CH_4 ($mol \cdot L^{-1} \cdot atm^{-1}$).

For CO_2, due to the complexity of the CO_2/DIC system, an "extraction efficiency" was defined as the proportion of inorganic carbon (as CO_2) in the headspace relative to the total inorganic carbon (DIC plus CO_2 gas) in the entire vial (1). The portion of this extraction efficiency affected by water volume alone, i.e., the extraction efficiency after acidification, was assumed to be proportional to the fractional volume of headspace in the jar. An exact relationship between fraction of headspace volume and the volume component of extraction efficiency (E_V) was determined by addition of 2 mM $NaHCO_3$ in volumes equal

to 25%, 50%, and 75% of the total vial volume to sealed vials with a headspace of N_2 at atmospheric pressure, followed by addition of excess H_3PO_4 and measurement of headspace CO_2 concentrations by GC-IRMS. This determination resulted in the following relationship:

$$E_V = -0.8057\left(\frac{V_{water}}{V_{vial}}\right) + 0.8458. \quad \textbf{[S2]}$$

In addition to the volume effect, acidification was required to extract the CO_2 into the headspace of some of the incubations with full efficiency, but the incubations were not acidified until the end of the incubation period. Therefore, the CO_2 concentrations measured over the course of the incubations had to be corrected for a pH component of extraction efficiency in addition to the volume component. The pH component of the extraction efficiency (E_{pH}) is defined as

$$E_{pH} = \frac{n^{before}_{CO_2,HS}}{n^{after}_{CO_2,HS}}, \quad \textbf{[S3]}$$

where $n^{before}_{CO_2,HS}$ is the amount of CO_2 in the headspace before acidification (mol) and $n^{after}_{CO_2,HS}$ is the amount of CO_2 in the headspace after acidification (mol). Although the incubations were only acidified on the final day, the pH of selected incubations was measured before acidification and found to be close to the in situ pH measured in the field, so E_{pH} was assumed to be constant throughout the incubation period. The value $E_{pH} = 1$ was used for the incubations that experienced no significant change in headspace CO_2 concentration after acidification. The total extraction efficiency for CO_2 (E_{total}) is the product of the volume and pH components,

$$E_{total} = E_V E_{pH}, \quad \textbf{[S4]}$$

and the total amount of inorganic carbon in the entire vial (n_{CO_2}) is then the amount of CO_2 in the headspace (calculated analogously to the amount of headspace CH_4) divided by the total extraction efficiency:

$$n_{CO_2} = \frac{\chi_{CO_2} P(V_{vial} - V_{water})}{RT}\frac{1}{E_{total}}. \quad \textbf{[S5]}$$

In addition to the effect of pH on the total CO_2 extraction efficiency, pH also had a slight effect on the measured $\delta^{13}C_{CO2}$ values. Therefore, in addition to the correction for $E_{pH} < 1$, these incubations were also corrected to account for these shifts in $\delta^{13}C_{CO2}$ with acidification:

$$\delta^{13}C^{corr}_{CO_2} = \delta^{13}C^{meas}_{CO_2} + \left(\delta^{13}C^{after}_{CO_2} - \delta^{13}C^{before}_{CO_2}\right), \quad \textbf{[S6]}$$

where $\delta^{13}C^{corr}_{CO_2}$ is the corrected value, $\delta^{13}C^{meas}_{CO_2}$ is the measured value, $\delta^{13}C^{after}_{CO_2}$ is the measured value after acidification, and $\delta^{13}C^{before}_{CO_2}$ is the measured value before acidification.

Measured amounts and $\delta^{13}C$ of CH_4 and CO_2 over the incubation period are shown in Fig. S1. CH_4 and CO_2 production rates were calculated based on linear regressions of molar amount (corrected for extraction efficiency) per gram of dry peat vs. time. To quantify changes in CH_4 and CO_2 production along the thaw progression, we assigned numbers 1–9 to the sites based on the hypothesized order of the thaw succession (Table 1 and Table S1) and performed linear regressions on the base-10 logarithms of the CH_4 and CO_2 production potentials and ratios in the individual incubation replicates vs. thaw position (Fig. S2). The logarithms of the production potentials were used due to the nonlinearity of the increase in gas production rates with thaw (Fig. 1 *A* and *B*), and the logarithms of CH_4/CO_2 ratios were used because the ratio of two exponential functions is also exponential. Statistical significance was tested based on the correlation coefficients (R^2) of the regressions, and all increases were found to be significant with $P < 0.0001$.

Overall $\delta^{13}C_{CH4}$ and $\delta^{13}C_{CO2}$ for the incubation period (Fig. 2 *A* and *B*) were defined as the acidification-corrected $\delta^{13}C_{CH4}$ and $\delta^{13}C_{CO2}$ on day 62 (which represent integrated $\delta^{13}C$ of all gas production during the incubations), and α_C values (2) were calculated based on these corrected final $\delta^{13}C$ values. The incubations appeared to fall into two groups based on α_C (Fig. 2*C*): group 1 consisting of collapsed palsas and bogs ($\alpha_C = 1.085 \pm 0.001$), and group 2 consisting of all fens ($\alpha_C = 1.052 \pm 0.001$). Based on an independent two-sample unpaired *t* test, the groups were significantly different with $t(24) = 16.5564$ and $P < 0.0001$.

C/N ratios. Five to 10 g of each peat core section was weighed, dried at 60 °C until completely dry (3–10 d), weighed again, and ground to a fine powder. For each peat depth, two subsamples—one 80–100-μg subsample for C analysis and one 5,000–6,000-μg subsample for N analysis—were wrapped in tin capsules. Samples were analyzed by combustion to CO_2 and N_2 at 1,020 °C in an automated CHN elemental analyzer coupled with a Thermo-Finnegan Delta XP isotope ratio mass spectrometer. Samples were run in nondilution mode for carbon analysis and dilution mode (×10) for nitrogen analysis.

Results were obtained in the form of %C and %N (by weight), and the C/N ratios were calculated as the ratio of %C/%N for corresponding pairs of subsamples.

FTIR Spectroscopy. Spectral characterization of peat samples was performed by diamond attenuated total reflectance FTIR spectroscopy on a PerkinElmer Spectrum 100 FTIR spectrometer fitted with a CsI beam splitter and a deuterated triglycine sulfate detector. An attenuated total reflectance (ATR) accessory made from a composite of zinc selenide and diamond, with a single reflectance system, was used to produce transmission-like spectra. Peat samples were first dried in an oven at 60 °C until completely dry (3–10 d), then ground to a fine powder. Samples were then placed directly on the crystal and force was applied to ensure good contact between the crystal and the sample. Spectra were acquired by averaging 50 scans at 4-cm^{-1} resolution (wavenumber) over the range 4,000–650 cm^{-1}. The spectra were corrected for the ATR to allow for differences in depth of beam penetration at different wavelengths, and then baseline corrected, with the instrument software.

To calculate humification indices, we calculated ratios between absorbances at the following wavenumbers with respect to polysaccharides (1,030 cm^{-1}): 2,920, 2,850, 1,630, and 1,515 cm^{-1} (3–6) (functional group assignments for each wavenumber are given in Fig. 4*B*). Beer et al. (5) and Broder et al. (6) define the polysaccharide and aromatic C=C/amide C=O wavenumbers as 1,090 cm^{-1} and 1,510 cm^{-1}, respectively, but the corresponding absorption maxima in our samples occur closer to 1,030 cm^{-1} and 1,515 cm^{-1}.

FT-ICR MS. A custom-built FT-ICR mass spectrometer with 9.4-T superconducting magnet located at the National High Magnetic Field Laboratory (NHMFL) was used to collect ultrahigh resolution mass spectra in two selected pore water samples: one from the SOS site at 31 cm, and one from the E site at 25.5 cm. The use of this instrument to determine the composition of complex natural dissolved organic matter in peatland porewaters has been described in detail (7, 8). Briefly, a solution containing the dissolved organic matter (DOM) in methanol was prepared for each selected sample by solid phase extraction (9) so that the final concentration was 500 mg C/mL. Samples were then introduced

to an electrospray ionization source through a syringe pump at a flow rate of 0.5 μL/min that was equipped with a 50-μm i.d. fused silica tube (10, 11). Two hundred individual scans were summed and the average resolving power (m/Dm 50%) was >700,000 at 451 Da. Spectra were calibrated by two internal series of DOM homologous series separated by 14 Da ($-CH_2$ groups) and the mass accuracy was calculated to be <1 ppm for singly charged ions ranging across the mass spectral distribution (m/z 300–900). NHMFL MS software was used to calculate all possible molecular formulas within a ±1-ppm error taking into consideration the presence of C, H, O, N, and S (12). All observed ions were singly charged as confirmed by the 1.0034-Da spacing found between isotopic forms of the same molecule (between $^{12}C_n$ and $^{12}C_{n-1}{}^{13}C_1$) (13, 14).

1. Corbett JE, et al. (2013) Partitioning pathways of CO_2 production in peatlands with stable carbon isotopes. *Biogeochemistry* 114(1-3):327–340.
2. Whiticar MJ, Faber E, Schoell M (1986) Biogenic methane formation in marine and freshwater environments: CO_2 reduction *vs.* acetate fermentation—Isotope evidence. *Geochim Cosmochim Acta* 50(5):693–709.
3. Holmgren A, Nordén B (1988) Characterization of peat samples by diffuse reflectance FT-IR spectroscopy. *Appl Spectrosc* 42(2):255–262.
4. Niemeyer J, Chen Y, Bollag J-M (1992) Characterization of humic acids, composts, and peat by diffuse reflectance Fourier-transform infrared spectroscopy. *Soil Sci Soc Am J* 56(1):135–140.
5. Beer J, Lee K, Whiticar M, Blodau C (2008) Geochemical controls on anaerobic organic matter decomposition in a northern peatland. *Limnol Oceanogr* 53(4):1393–1407.
6. Broder T, Blodau C, Biester H, Knorr KH (2012) Peat decomposition records in three pristine ombrotrophic bogs in southern Patagonia. *Biogeosciences* 9(4):1479–1491.
7. Tfaily MM, Podgorski DC, Corbett JE, Chanton JP, Cooper WT (2011) Influence of acidification on the optical properties and molecular composition of dissolved organic matter. *Anal Chim Acta* 706(2):261–267.
8. Tfaily MM, et al. (2013) Investigating dissolved organic matter decomposition in northern peatlands using complimentary analytical techniques. *Geochim Cosmochim Acta* 112:116–129.
9. Tfaily MM, Hodgkins S, Podgorski DC, Chanton JP, Cooper WT (2012) Comparison of dialysis and solid-phase extraction for isolation and concentration of dissolved organic matter prior to Fourier transform ion cyclotron resonance mass spectrometry. *Anal Bioanal Chem* 404(2):447–457.
10. Chowdhury SK, Katta V, Chait BT (1990) An electrospray-ionization mass spectrometer with new features. *Rapid Commun Mass Spectrom* 4(3):81–87.
11. Senko MW, et al. (1996) Electrospray ionization Fourier transform ion cyclotron resonance at 9.4 T. *Rapid Commun Mass Spectrom* 10(14):1824–1828.
12. Stenson AC, Marshall AG, Cooper WT (2003) Exact masses and chemical formulas of individual Suwannee River fulvic acids from ultrahigh resolution electrospray ionization Fourier transform ion cyclotron resonance mass spectra. *Anal Chem* 75(6): 1275–1284.
13. Brown TL, Rice JA (2000) Effect of experimental parameters on the ESI FT-ICR mass spectrum of fulvic acid. *Anal Chem* 72(2):384–390.
14. Kujawinski EB, Hatcher PG, Freitas MA (2002) High-resolution Fourier transform ion cyclotron resonance mass spectrometry of humic and fulvic acids: Improvements and comparisons. *Anal Chem* 74(2):413–419.

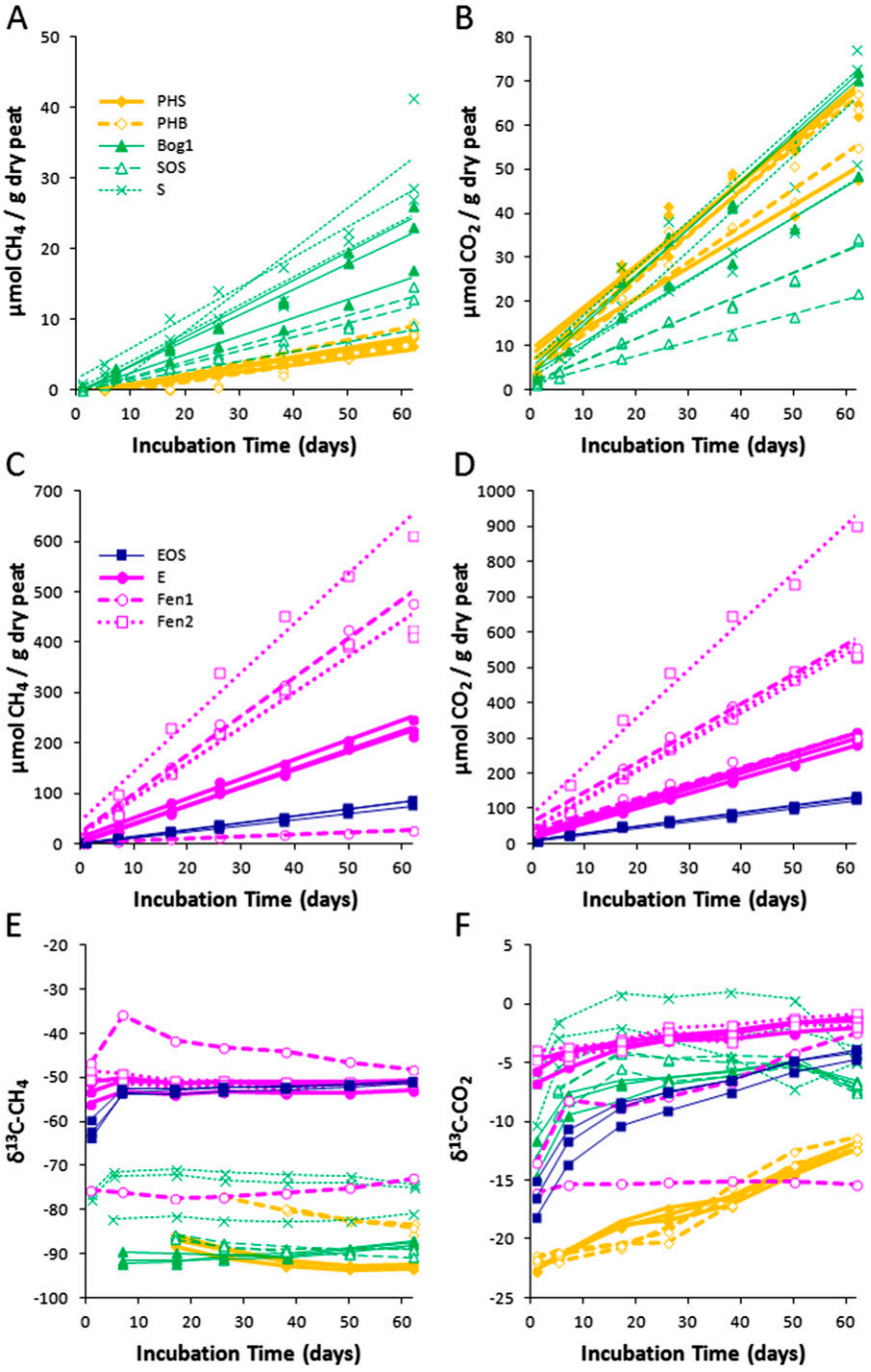

Fig. S1. Cumulative amounts and $\delta^{13}C$ of CH_4 and CO_2 produced in incubations. (*A–D*) Amounts of CH_4 and CO_2 produced in peat from collapsed palsas (gold: PHS, PHB), bogs (green: Bog1, SOS, S), fens with *Sphagnum* spp. and sedges (dark blue: EOS), and fens with sedges only (pink: E, Fen1, Fen2), overlaid with linear fits used to calculate gas production rates (R^2 = 0.84–1.00). Lines of the same style represent incubation replicates. (*E* and *F*) $\delta^{13}C$ of CH_4 and CO_2 in all incubations, connected with lines to show overall trends (same marker and line styles as *A–D*). Within-sample error bars are smaller than the marker sizes.

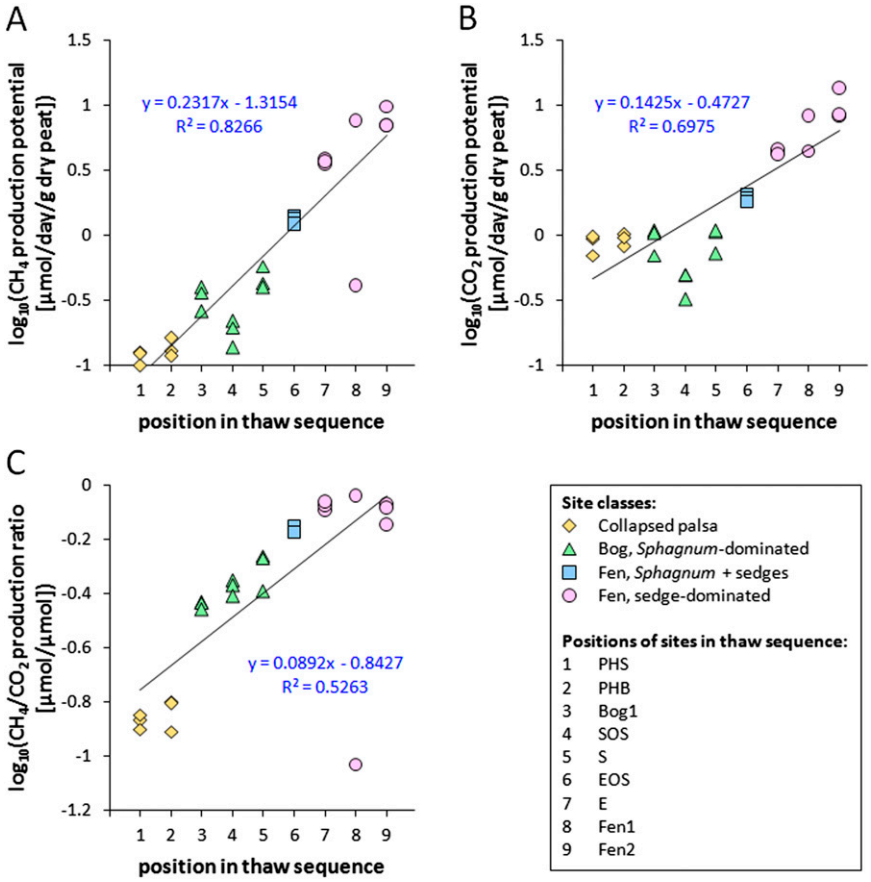

Fig. S2. Log-linear regressions of incubation-derived gas production potentials vs. position in the thaw sequence: (*A*) CH_4 production potential, (*B*) CO_2 production potential, and (*C*) CH_4/CO_2 production ratio. "Position in thaw sequence" is defined as the approximate order of time since permafrost thaw for the sites used in this study (see the first footnote in Table S1).

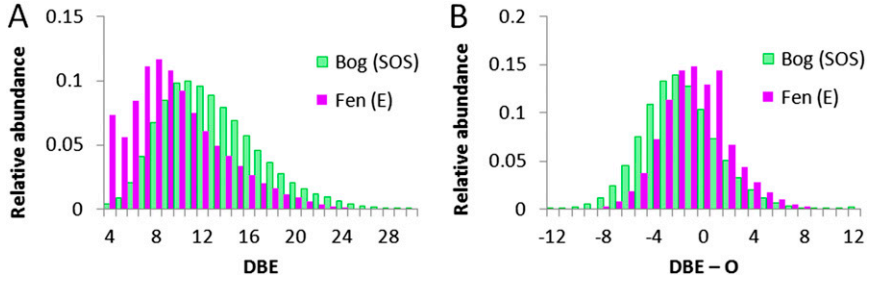

Fig. S3. Abundance distributions of compounds in DOM as a function of double-bond equivalence (DBE) and DBE–O. The leftward shift of the bog (site SOS, 31 cm) relative to the fen (site E, 25.5 cm) distribution between (*A*) DBE and (*B*) DBE–O, together with bog DOM's higher O/C ratios (Fig. 5*A*), indicates higher oxygen content in bog DOM. This result signifies that bog DOM has a higher oxidation state than fen DOM.

Table S1. Sites selected for study, in approximate order of thaw stage

Site name*	Habitat classification	Dominant vegetation	pH‡	WTD, cm§	Thaw depth, cm¶	"Surface" depths used for incubations, cm	Notes
PHS	Collapsed palsa	*Eriophorum vaginatum*, woody species	4.1	0	>90	9–12	Smaller thermokarst sinkhole.
PHB	Collapsed palsa	*E. vaginatum*, floating *Sphagnum*	4.1	>0	>90	10–15	Larger thermokarst sinkhole.
Bog1	Bog	*Sphagnum* spp.	4.2	−17	25	18–22	Elevation close to surrounding palsa.
SOS	Bog	*Sphagnum* spp.	4.0	−12	34	12–17	Intermediate between Bog1 and S.
S (triplicate cores)†	Bog	*Sphagnum* spp.	4.2	−12 to −13	30–31	12–16	Thawed much deeper than Bog1 or SOS in August 2012.
EOS	Fen	*Eriophorum angustifolium*, *Sphagnum* spp.	4.8	5	44 to >90	5–10	Sporadic, thin frozen layer at 44 cm.
E (triplicate cores)†	Fen	*E. angustifolium*	5.8	0–4.5	27 to >90	5–8	Usually thaws completely by August.
Fen1	Fen	*Carex rostrata*	6.0	6–8	>90	5–8	Usually thaws completely by August.
Fen2	Fen	*E. angustifolium*	5.7	12	>90	0–10	Usually thaws completely by August.

Expanded from Table 1 to include water table depth (WTD), thaw depth, depths used for incubations, and additional information.

*Order of sites determined by habitat classification (see main text), vegetation, active layer depth, WTD, and in the case of fens, distance from the nearest lake (Lake Villasjön), which has been gradually increasing in size with the thaw of surrounding permafrost.

†CH_4 and CO_2 fluxes (1) have previously been measured with an autochamber system at these sites.

‡Average pore water pH between 0 and 32 cm below peat surface. Within this depth range, pH did not show any appreciable trends with depth. SEs ≤ 0.15 pH units.

§Positive numbers indicate water above the peat surface (most common sign convention for WTD, which is opposite of other depths indicated).

¶Thaw depth at time of sampling. Actual active layer, which includes seasonally frozen peat, is thicker.

1. Bäckstrand K, et al. (2010) Annual carbon gas budget for a subarctic peatland, Northern Sweden. *Biogeosciences* 7:95–108.

Table S2. Humification indices (HI) of (*A*) surface peat from <10 cm, (*B*) near-surface peat from depths used in incubations (Table S1), and (*C*) deep peat from 24 to 35 cm.

Site	Depth, cm	2,920/1,030	2,850/1,030	1,630/1,030	1,515/1,030
Surface core sections, <10 cm					
PHS	1–4	0.64	0.52	0.53	0.20
PHB	0–5	0.54	0.43	0.34	0.11
Bog1	0–4	0.44	0.32	0.26	0.09
SOS	0–6	0.48	0.36	0.28	0.09
S	1–4	0.43	0.34	0.24	0.09
EOS	0–5	0.64	0.47	0.59	0.30
E	1–4	0.76	0.56	0.70	0.40
Fen1	1–4	0.42	0.32	0.36	0.18
Fen2	0–10*	0.57	0.45	0.44	0.21
Near-surface core sections, Table S1; used in incubations					
PHS	9–12	0.56	0.42	0.41	0.15
PHB	10–15	0.66	0.52	0.44	0.13
Bog1	18–22	0.48	0.37	0.33	0.13
SOS	12–17	0.45	0.36	0.26	0.09
S	12–16	0.51	0.40	0.34	0.14
EOS	5–10	0.88	0.67	0.71	0.33
E	5–8	0.64	0.48	0.55	0.28
Fen1	5–8	0.64	0.51	0.57	0.32
Fen2	0–10	0.57	0.45	0.44	0.21
Deep core sections, 24–35 cm					
PHS	30–33	0.56	0.43	0.48	0.20
PHB	25–30	0.78	0.61	0.49	0.21
Bog1	27–31	0.66	0.50	0.46	0.19
SOS	27–33	0.72	0.56	0.41	0.16
S	17–21†	0.57	0.42	0.36	0.15
EOS	25–30	1.09	0.86	0.88	0.47
E	24–27	0.57	0.41	0.42	0.21
Fen1	24–27	1.64	1.15	1.02	0.60
Fen2	30–35	0.86	0.71	0.75	0.41

Within-sample variability for all HI is ±0.01 (SE), based on parallel analysis of replicate samples collected at the same depth and time.

*Same as incubation sample.

†No samples were gathered deeper than 21 cm at this site. Because this section was from above 24 cm, these values are not shown in Fig. 3*B*.